Impact of DME/TACAN on GNSS L5/E5a Receivers at Low Altitude Considering Multipath

Nicolas Gault, Axel Javier Garcia Peña, Alexandre Chabory, Christophe Macabiau

Impact of DME/TACAN on GNSS L5/E5a Receivers at Low Altitude Considering Multipath

Nicolas Gault, *École Nationale de l'Aviation Civile (ENAC)*
Axel Garcia-Pena, *École Nationale de l'Aviation Civile (ENAC)*
Alexandre Chabory, *École Nationale de l'Aviation Civile (ENAC)*
Christophe Macabiau, *École Nationale de l'Aviation Civile (ENAC)*

Biographies

Nicolas GAULT graduated as a space and aeronautical telecommunications engineer from ENAC (École Nationale de l'Aviation Civile) in 2020, Toulouse, France. He is now a Ph.D student at the TELECOM lab of ENAC. His Ph.D topic deals with the model of impact of interferences on the GNSS L5/E5a band.

Axel GARCIA-PENA is a researcher/lecturer with the SIGnal processing and NAVigation (SIGNAV) research axis of the TELECOM lab of ENAC (French Civil Aviation University), Toulouse, France. His research interests are GNSS navigation message demodulation, optimization and design, GNSS receiver design and GNSS satellite payload. He received his double engineer degree in 2006 in digital communications from SUPAERO and UPC, and his PhD in 2010 from the Department of Mathematics, Computer Science and Telecommunications of the INPT (Polytechnic National Institute of Toulouse), France.

Alexandre CHABORY received the M.Sc. degree in electrical engineering from ENAC, the French Civil Aviation University, Toulouse, in 2001, and the Ph.D. degree from Paul Sabatier University, Toulouse, in 2004. From 2004 to 2007, he was a Post-Doctoral Scientist with the Eindhoven University of Technology, the Netherlands. Since 2007, he has been with ENAC where he is now full-professor and heading the electromagnetics and antennas research group. His research interests include electromagnetic theory and modeling, mainly for aeronautical applications.

Christophe MACABIAU graduated as an electronics engineer in 1992 from the ENAC (Ecole Nationale de l'Aviation Civile) in Toulouse, France. Since 1994, he has been working on the application of satellite navigation techniques to civil aviation. He received his Ph.D in 1997 and has been in charge of the signal processing lab of ENAC since 2000, where he also started dealing with navigation techniques for terrestrial navigation. He is currently the head of the TELECOM team of ENAC, that includes research groups on signal processing and navigation, electromagnetics, and data communication networks.

Abstract

In the context of civil aviation, GNSS L5/E5a Radio Frequency Interference (RFI) environment is dominated by pulsed interferences such as JTIDS/MIDS and DME/TACAN causing a degradation of the effective C/N_0 observed by the receiver. The mitigation of the pulse RFI as well as its precise characterization is fundamental to guarantee the provision of the civil aviation Safety-of-Life service, as depicted in (Garcia-Pena, Macabiau, et al., 2020). In order to mitigate the pulsed RFI impact, in civil aviation standards, a temporal blanker is used as a counter measure. The effective C/N_0 is thus computed accounting for the temporal blanker introduction through the derivation of the blanker duty cycle, bdc, and the equivalent noise level contribution of the non-blanked interference, R_I.

However, none of the characterizations found in the scientific literature or in the standards considers any multipath effect. This effect is especially important at low altitude since the airborne GNSS receiver could be significantly affected by echoes created by low altitude obstacles, potentially increasing bdc and R_I. Therefore, in this work, it is proposed to update the mathematical model of the effective C/N_0 with the introduction of multipath.

The introduction of this new model is used to compare the impact of multipath at low and at high altitude flight levels (FL). The comparison is conducted in two parts in this work. First, an analysis shows that to increase the blanking duty cycle by 50%, the size

of an obstacle should be four times larger when the aircraft is at high altitude FL in comparison with low altitude FL. Second, an analysis of a potential low altitude hot-spot located at JALTO, Philadelphia, shows that the impact of multipath must not be neglected; nevertheless, it is shown that the low altitude hot spot exceeding the existing worst-case scenario at FL400 is highly unlikely.

1. INTRODUCTION

The nominal processing of GNSS received signals can be affected by noise as well as received additive signals such as multipath and Radio Frequency Interference (RFI). RFI sources are of various sorts and their impact depends on the user application. In the context of civil aviation, Global Navigation Satellite System (GNSS) L5/E5a interference environment is dominated by pulsed interferences such as DME/TACAN and JTIDS/MIDS. A long thread of activities led or are leading to the elaboration of various ICAO, RTCA and EUROCAE standards to determine and to bound the vulnerability of airborne GNSS receivers equipped with their relevant antenna in the L5/E5a band to these RFI sources. In these standards, the RFI impact on a GNSS receiver is well characterized as the C/N_0 degradation observed at the receiver's correlator output, or equivalently, as an increase of the effective N_0 denoted as $N_{0,eff}$.

In civil aviation, $N_{0,eff}$ is computed taking into account the presence of temporal blanker in the receiver Radio Frequency Front-End (RFFE) block, as depicted in the RTCA DO-292, (2004). The role of the blanker is to set to zeros the samples whenever the instantaneous power envelope of a received pulse is higher than a certain threshold. Depending on the DME/TACAN interfering scenarios (number of beacons, received power at the aircraft level, pulses time of arrival etc.), the value of bdc (percentage of samples set to zero by the blanker) and R_I (the below-blanker interfering-signal-to-thermal-noise ratio) can be determined and the $N_{0,eff}$ computed. A worst-case scenario was found in RTCA DO-292, (2004) at Harrisburg P.A, high altitude (FL400), where the C/N_0 degradation due to DME/TACAN only is up to 5.99 dB. Note that this value is to be updated in the RTCA DO-292A since an interpretation error have been found in the RTCA, (2004) and confirmed by the RTCA SC-159 WG6.

However, none of the previous characterizations consider any multipath effect which is especially important at low altitude Flight Level (FL) since the airborne GNSS receiver could be significantly affected by echoes created by low altitude obstacles. Indeed, the echoed pulses would impact the receiver in the same manner as the direct pulses: echoed pulses could trigger the temporal blanker and thus increase the value of bdc or could just increase the overall R_I value. As a result, new R_I and bdc formulas have to be derived to correctly consider multipath in the $N_{0,eff}$ computation; these formulas must tackle the collision of echoes with the direct signal pulses as well as the collision of echoes generated by other obstacles, knowing that the collision can distort the original shape of the DME/TACAN and JTIDS/MIDS pulses, highly complexifying the analysis. Furthermore, these new formulas require the knowledge of the precise time of arrival of the echoed pulses as well as their received power at the aircraft level. Therefore, a propagation channel model specially adapted for DME/TACAN interference analysis had to be developed. However, the newly developed RFI-focuses propagation channel model should be as simple as possible (as opposite to highly resource consuming propagation channel models) to allow its application to complex scenarios (high number of obstacles, such as real 2D/3D maps) while still being representative from a RFI impact point of view.

The general objective of this paper is thus to first present new R_I and bdc formulas considering multipath, second to present a DME/TACAN multipath interference propagation channel and third, to present two meaningful numerical examples of the proposed new formulas and propagation channel model. The first example is a comparison of the area necessary to increase bdc by 50%, at low and at high altitude FL. The second example is the study of a potential low altitude FL US operational hot spot, JALTO, Philadelphia, determined during RTCA SC-159 WG6 activities.

Following this three-fold objective, the paper is organized as follows. In the first section, the DME/TACAN signal and system are presented. The second section presents the RTCA DO-292, (2004) analytical model for the multipath-free effective C/N_0 calculation, as well as its application to the US worst-case scenario (US FL400 hot spot). In the third section, the bdc and R_I mathematical models including multipath impact are introduced. The fourth section introduces the proposed propagation channel model adapted to interference calculations purposes. The sixth section presents the two numerical examples of the application of the new propagation channel model and the R_I and bdc formulas.

2. DME/TACAN SIGNAL AND SYSTEM DESCRIPTION

DME, and its military equivalent, TACAN, are two systems used by aircrafts to determine their distance to a ground station, whose position is known. The systems operate as follows. The aircraft DME equipment, called interrogator, sends pulses to ground stations. Once the interrogation is detected, the station transponder replies to the interrogator. The distance is then determined by measuring the time elapsed between each pulse transmitted by the interrogator and the reception of its corresponding reply pulse from the transponder. This delay corresponds to twice the distance between the aircraft and the station, as well as a fixed processing time inside the ground station.

According to the RTCA DO-292, (2004) only the signals emitted in the band of interest of the study disturb GNSS receivers operations, the band of interest being the E5a/L5 one, equal to [1164 MHz; 1191 MHz]. The aircraft's DME interrogators emitting their signals between 1025 and 1151 MHz or between 1191 MHz and 1215 MHz, they are ignored herein. The study focuses on DME ground stations, as they emit their signals between 962 and 1213 MHz, which includes the defined band of interest defined above.

The emitted signal of an individual DME station is composed of a pair of Gaussian pulses modulated by a cosine, which can be modelled as:

$$s(t) = \sqrt{2P}\sum_{k=1}^{K}\left(e^{-\frac{\alpha(t-t_k)^2}{2}} + e^{-\frac{\alpha(t-\Delta_t-t_k)^2}{2}}\right)\cos\left(2\pi f_i t + \theta_i\right) \quad (1)$$

Where:

- P is the interference beacon transmitting peak envelope power (dBW),
- $\alpha = 4.5 \cdot 10^{11} s^{-2}$ is a constant of pulse,
- Δ_t = 12 μs is the inter pulse time separation,
- t_k is the emission time of the k^{th} pulse pair,
- f_i is the carrier frequency of the DME/TACAN signal (Hz),
- θ_i is the DME/TACAN signal initial carrier phase shift.

Note that Equation (1) has been corrected from previous publications of the authors to define P as the Peak Envelope Power (PEP) instead of as an Instantaneous Peak Power (IPP). Definition of P as peak envelope power leads to a more consistent definition since DME specifications are provided with a PEP values. From Equation (1), instantaneous power of a single pulse, $p(t)$, can be defined:

$$p(t) = Pe^{-\alpha t^2} \quad (2)$$

Where

- P is the peak envelope power (PEP) of the pulsed interfering source at the antenna output.

Figure 1 (left part) represents a normalized DME/TACAN pulse pair, modulated at 14 MHz. **Figure 1** (right part) represent the normalized pulse complex envelope of a DME/TACAN signal.

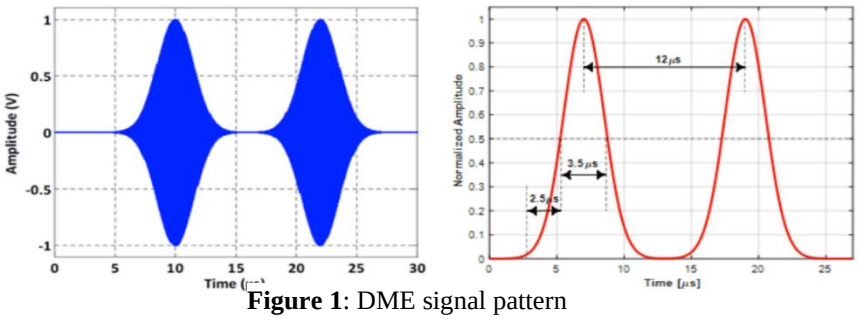

Figure 1: DME signal pattern

3. RTCA DO-292 MULTIPATH-FREE C/N_0 DEGRADATION MODEL

In this section, the general analytical multipath-free C/N_0 degradation model, and the mathematical multipath-free bdc and R_I models are presented. Using these models, the value of the C/N_0 degradation due to DME/TACAN only at the US FL400 hot spot without considering multipath is derived.

3.A. GENERAL ANALYTICAL MODEL

In order to understand the DO-292 degradation analytical model, a generic civil aviation GNSS receiver structure as well as the behavior and effect of its components on the received signals are described. The receiver structure is presented in **Figure 2**.

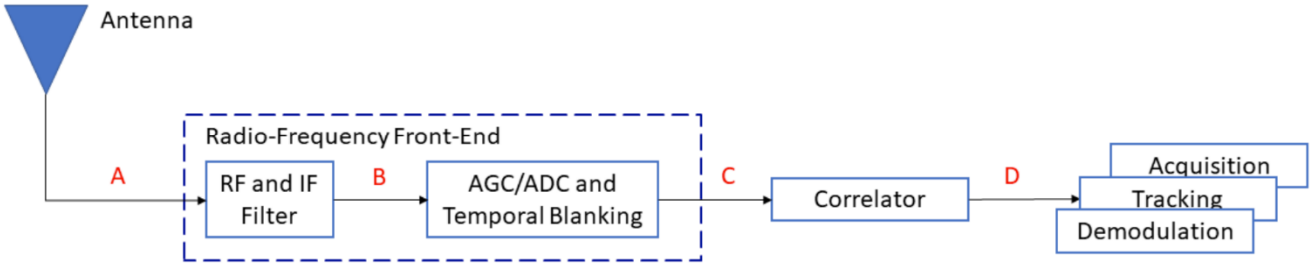

Figure 2: Generic civil aviation GNSS receiver block scheme

First, the antenna is the element responsible of capturing the incoming signal: at the antenna port (point A), there is a mix of all incoming signals; useful signals, GNSS and SBAS signals, and RFI signals such as DME/TACAN, JTIDS/MIDS, etc. Once the signals have been captured by the antenna, they are passed to the Radio-Frequency Front End (RFFE) block. This block amplifies the received signals, shifts them from their received signal frequency carrier to the intermediate frequency and filters them. The filtered signals are modelled in **Figure 2** at the RF (Radio-Frequency) and IF (Intermediate Frequency) filters output at point B. The joint effect of these two filters and the antenna filtering are defined by RTCA, (2004)with an equivalent filter whose transfer function is provided **Figure 3**.

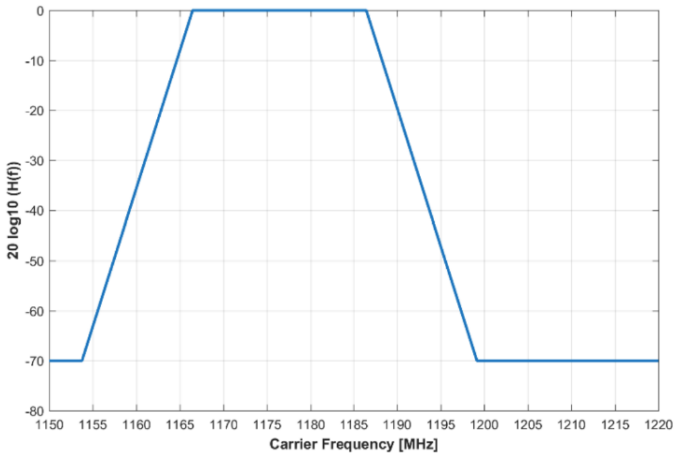

Figure 3: Radio Frequency Front-End plus antenna equivalent transfer function defined in RTCA DO-292, BW = 20MHz

The RFFE block is also responsible for digitizing the filtered signals with the application of the ADC (Analog-Digital-Converter) coupled with the AGC (Automatic-Gain-Control). For a civil aviation receiver, the temporal blanker is introduced at that point. The temporal blanker is a device which blanks (put to 0s) the time samples of the incoming signal (mix of signals) which are over a threshold; the digitized and blanked signal is found at point C. In the RTCA, (2004), the defined blanker is an instantaneous blanker. This blanking method removes all the time samples of the incoming signal which have an envelope power over a given threshold. For an optimal functioning, the blanker should also be coupled with the ADC/AGC blocks: to ensure that high-power signals are not saturating the ADC/AGC and that the blanked signal spans the ADC quantization range. **Figure 4** presents an example of the RTCA, (2004) instantaneous blanker.

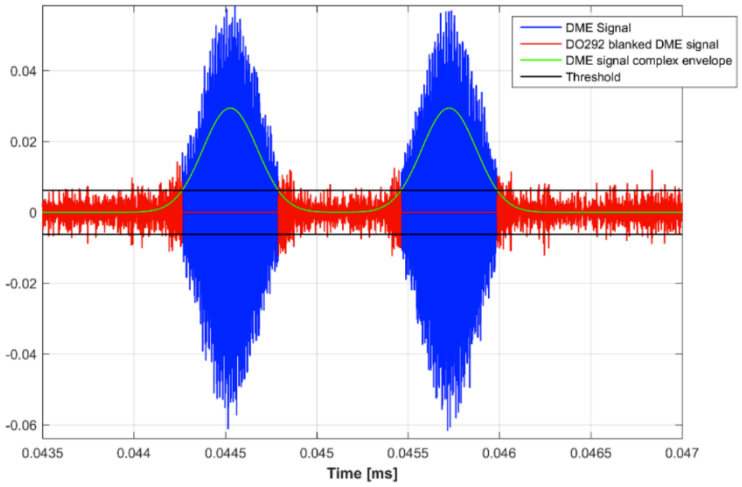

Figure 4: Example of the behavior of the DO-292 instantaneous blanker over the signal complex envelope

Note that limitations about this blanking method have been assessed in Garcia-Pena et al., (2019).

Finally, digitized and blanked signals are fed to the correlator. The impacts of the RFI signals and blanking method are measured at the output of the correlator (point D). The chosen figure of merit is the signal C/N_0; or more specifically, the difference between the C/N_0 when only the useful signal is present at the receiver antenna port (no RFI signals) and the C/N_0 when the useful signal and RFI signals are present at the receiver antenna port, also called effective C/N_0 or $C/N_{0,eff}$. Note that the difference between these two C/N_0 values is also called the degradation introduced by the RFI signals.

Although the blanking method is going to affect the power of the useful signal (part of the signal is removed and its power is decreased), RTCA DO-292 proposes to model the $C/N_{0,eff}$ by defining an equivalent $N_{0,eff}$. $N_{0,eff}$ represents the effective noise power spectrum density that a receiver will observe at the correlator output if the receiver captures a useful signal with power C at the correlator output and no RFI signals are present. In other words, RTCA DO-292 proposes a generic formula to compute the degradation of the C/N_0 through the increase of the background noise due to pulsed and continuous RFI.

In order to mathematically model $N_{0,eff}$, the following points about the impact of pulsed RFI signals on $N_{0,eff}$ must be considered:

- Part of the signal is removed due to the blanker. Since the impact on the useful signal power $(1 - bdc)^2$ is higher than the impact on the power of the noise$(1 - bdc)$, the equivalent $N_{0,eff}$ is increased by a factor of $1/(1 - bdc)$. bdc is the blanker duty cycle, or in other words, the percentage of time the incoming signal is blanked ($bdc \in [0,1]$).
- Not all the RFI signal samples have a power above the threshold; therefore, there is a part of the RFI signal that is not removed, and its influence must be added to the below-threshold interfering-signal-to-thermal-noise ratio, R_I.

With these considerations, the mathematical model proposed by the RTCA DO-292 for $N_{0,eff}$ is:

$$N_{0,eff} = \frac{N_O}{(1 - bdc)} \cdot (1 + \frac{I_{0,WB}}{N_0} + R_I) \quad (3)$$

Where:

- N_0 is the thermal noise power spectrum density level generated by the RFFE,
- bdc is the blanker duty cycle,
- $I_{0,WB}$ is the contribution of wideband (non-pulsed) signals to $N_{0,eff}$,
- R_I is the below-threshold interfering-signal-to-thermal-noise ratio.

The objective of this paper is to assess the impact of multipath considering DME/TACAN; therefore, for simplification purposes it is assumed that $I_{0,WB} = 0$, which yields:

$$N_{0,eff} = \frac{N_O}{(1 - bdc)} \cdot (1 + R_I) \tag{4}$$

And finally,

$$\left(\frac{C}{N_0}\right)_{deg} = 10\log_{10}\left(\frac{N_0}{N_{0,eff}}\right) = 10\log_{10}\left(\frac{1 - bdc}{1 + R_I}\right) \tag{5}$$

3.B. MULTIPATH-FREE DME/TACAN bdc MATHEMATICAL MODEL

In this subsection, the example of a single pulse is presented to introduce the mathematical notations necessary to define the (RTCA, 2004) multipath-free DME/TACAN bdc mathematical model. In particular, the definition of the above threshold pulse width pw is especially detailed since this factor will be later impacted by the introduction of multipath.

Figure 5 provides an example of a single above-threshold pulse.

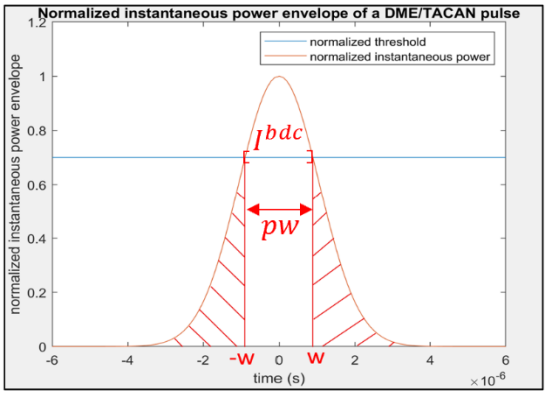

Figure 5*: Representation of an above-threshold DME/TACAN normalized pulse*

From **Figure 5**, three definitions are introduced:

- $-w$ and w are the instants of time where the pulse starts (stops) to be blanked. The mathematical expression of w is obtained by simply equalizing the pulse instantaneous power $p(t)$ (defined Equation (2)) to blanker threshold T_h:

$$p(w) = T_H \Leftrightarrow w = \sqrt{\frac{\ln\left({}^{P}/_{T_h}\right)}{\alpha}} \tag{6}$$

- I^{bdc} is the total blanked interval. From the definition of w, its mathematical expression is simply given by:

$$I^{bdc} = [-w, w] \tag{7}$$

- ***pw*** is the above threshold pulse width. From the expression of I^{bdc}, the mathematical expression of pw is as follows:

$$pw = length(I^{bdc}) = 2w \tag{8}$$

Note that the definition of pw is especially important since it will be impacted by the introduction of multipath.

Finally, from these definitions, RTCA DO-292 proposes a model for bdc specially adapted for DME/TACAN, derived from queuing theory, accounting for N pulses:

$$bdc = 1 - e^{-2\sum_{i=1}^{N} \boldsymbol{pw_i} \cdot PRF_i} \quad (9)$$

Where:

- N is the total number of sources, $N = N_D + N_T$ with N_D and N_T being the number of DME and TACAN respectively,
- PRF_i is the beacon pulse repetition frequency of source i, 2700 for DME and 3600 for TACAN

3.C. MULTIPATH-FREE DME/TACAN R_I MATHEMATICAL MODEL

In this subsection, first the multipath-free DME/TACAN mathematical model proposed by the (RTCA, 2004) is introduced. In particular, the definition of the below threshold equivalent pulse width PW is provided in detail for below and above blanker pulses, since its value will be directly impacted later by the introduction of multipath. Finally, a more accurate model for the multipath-free R_i mathematical model, proposed by Garcia-Pena, Julien, et al., (2020) is introduced.

From Equation (1), the multipath-free mathematical model of R_I proposed by RTCA DO-292 is introduced:

$$R_I = \sum_{i=1}^{N} \frac{P_i \boldsymbol{PW_i} PRF_i}{N_0 BW} \quad (10)$$

Where:

- BW is the RFFE filter bandwidth,
- N_0 is the thermal noise power spectrum density level generated by the RFFE,
- $\boldsymbol{PW_i}$ is the below threshold equivalent pulse width of a pair of pulse, such that:

$$PW_i = 2 \cdot PW_{i,pulse} \quad (11)$$

- $PW_{i,pulse}$ is the below threshold equivalent pulse width of a **single** pulse.

$PW_{i,pulse}$ can be seen as the width of an equivalent (in energy) rectangular pulse to the original RFI pulse (in this case, DME or TACAN) having the same peak envelope power P as the initial pulse. Equalizing the energy expressions of this rectangular equivalent pulse and the initial pulse yields:

$$PW_{i,pulse} = \frac{1}{P_i} \int_{-\infty}^{\infty} p(t)dt \quad (12)$$

Where $p(t)$ is the instantaneous power of one pulse as expressed in Equation (2). **Figure 6** provides an example for $PW_{i_{pulse}}$ for both a DME/TACAN below and above threshold pulse.

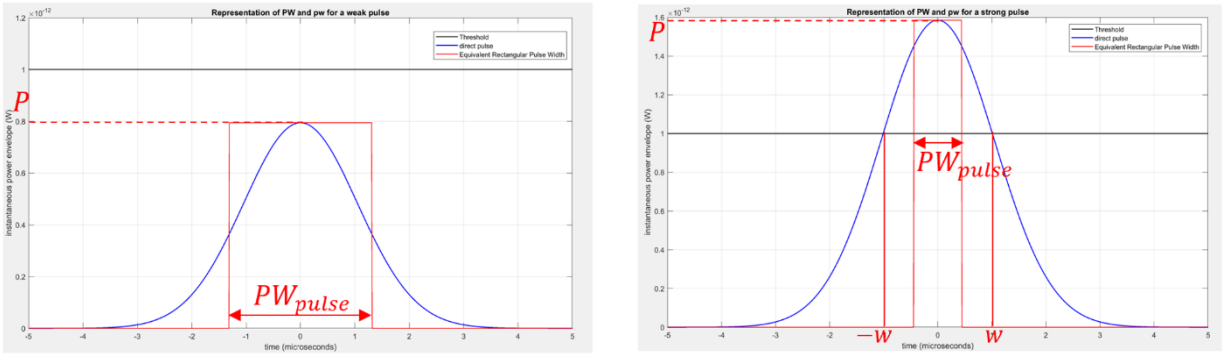

(a) (b)

Figure 6: Representation of DME/TACAN (a) weak pulse and (b) strong pulse

From **Figure 6**, two different cases must be distinguished to derive $PW_{i,pulse}$:

- Case (a): the pulse is below the threshold. By applying the Gaussian integral, we obtain:

$$PW_{i,pulse} = \frac{1}{P_i}\int_{-\infty}^{\infty} p(t)dt = \int_{-\infty}^{\infty} e^{-\alpha t^2}dt = \sqrt{\pi/\alpha} \tag{13}$$

- Case (b): the pulse is only partially below the threshold. In that case, the blanked interval must be excluded from the derivation, and from $u = \sqrt{\alpha}t$ change of variable:

$$PW_{i,pulse} = \int_{-\infty}^{-w} e^{-\alpha t^2}dt + \int_{w}^{\infty} e^{-\alpha t^2}dt = \sqrt{\frac{\pi}{\alpha}}erfc(\sqrt{\alpha}w) \tag{14}$$

Where $erfc(x) = \frac{2}{\sqrt{\pi}}\int_x^{+\infty} e^{-u^2}du$ is the complementary error function.

It must be noted that the R_I model of Equation (10) assumes that the post-blanker RFI signal power spectrum density (PSD) is completely spread which is a loose approximation. A more accurate model has been recently proposed by (Garcia-Pena, Julien, et al., 2020) to better model the post-blanker pulsed RFI signal PSD since simulations showed that the blanked signal is far from having a perfectly spread PSD. The proposed model is as follows:

$$R_I = \sum_{i=1}^{N} \frac{P_i \boldsymbol{PW_i} PRF_i}{N_0 \beta_0} \cdot SSC(\Delta f_i) \tag{15}$$

Where:

- β_0 is the thermal noise power degradation due to RFFE filter and correlator,

$$\beta_0 = \int_{-\infty}^{\infty} |H_{RF}(f)|^2 \bar{S}_{cm}(f)df \tag{16}$$

- $H_{RF}(f)$ is the baseband transfer function of the equivalent RFFE plus antenna filter,
- $SSC(\Delta f_i)$ is the Spectral Separation Coefficient of the pulsed interfering source i,

$$SSC(\Delta f_i) = \int_{-\infty}^{\infty} \bar{S}_{i,PBf}(f - \Delta f_i)\bar{S}_{cm}(f)df \tag{17}$$

- $\bar{S}_{i,PBf}$ is the i^{th} baseband post-blanker filtered normalized interfering signal PSD,
- $\bar{S}_{cm}$ is the normalized local replica PSD of the m^{th} satellite,
- Δf_i is the difference between L5/E5a central frequency f_{L5} and carrier frequency of interfering source i.

Note that Equation (10) and (15). will be affected in the same manner by the introduction of multipath, through the computation of PW_i, which is one of the most important factors of the R_I derivation. Hence, for simplification purposes, we propose to only keep equation (15) for the rest of the article.

3.D. APPLICATION TO RTCA DO-292 US HOT-SPOT

Applying the multipath-free model for R_I (Equation (10)), bdc (Equation (9)) and for the C/N_0 degradation (Equation (5)), RTCA, (2004) members determined in 2004 a worst-case scenario concerning the C/N_0 degradation due to DME/TACAN only, at Harrisburg, Pennsylvania, at high-altitude (FL400). However, as mentioned in the introduction, the value of the C/N_0 degradation found in the RTCA DO-292 needs to be updated since an interpretation error of the R_I model (Equation (10)) have been reported during the RTCA SC-159 WG6 activities. Applying the proposed model (Equation (15)) at the exact same spot, the value obtained for bdc and R_I are 0.59 and 0.61. From these two values, the C/N_0 degradation at this hot spot due to DME/TACAN only is

precisely 7.34 dB. This value is important to remember and will be compared to a potential low altitude hot-spot at JALTO, Philadelphia, in section 6 of this article.

4. PROPOSED bdc AND R_I MATHEMATICAL MODELS CONSIDERING MULTIPATH

Multipath is impacting the value of the C/N_0 degradation (Equation (5)) by modifying the values of bdc (Equation (9)) and R_I (Equation (15)), through the modification of the above threshold pulse width pw (Equation (8)) and the below threshold equivalent pulse width PW (Equation (11)) respectively. The objective of this section is to define the pw and PW formulas considering multipath.

In this section, the assumptions concerning the pulse collisions and the new notations necessary to the definition of the new pw and PW formulas are presented. Then, the new formula for pw and PW are introduced. Finally, an important remark on the necessary parameters to be obtained from the propagation channel model to derive the pw and PW formulas is highlighted.

Figure 7 provides a graphical example of the multipath impact on PW and pw, where an echoed pulse (in green) collides on the right of direct pulse (in red).

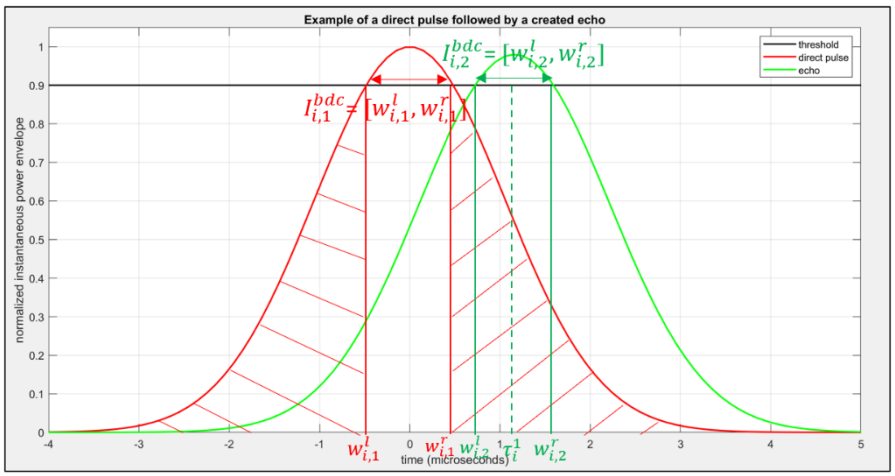

Figure 7: Representation of a direct DME/TACAN pulse followed by a created echo

4.A. PULSE COLLISION ASSUMPTIONS

As mentioned in the Introduction, the new formulas for R_I and bdc must tackle the collision of echoes with the direct signal pulses as well as the collision of echoes generated by other obstacles, knowing that the collision can distort the original shape of the DME/TACAN and JTIDS/MIDS pulses, highly complexifying the analysis. In this subsection, two assumptions concerning the pulse collisions, on the phase difference between pulses, and on the impact of the echoes generated by the first pulse on the second pulse of a pair of pulse, are presented to simplify the overall derivation.

Phase difference: The phase difference between two echoed pulses (or an echoed pulse and the LOS pulse) is modeled as a random uniform variable on $[0,2\pi]$. With this assumption, it can be shown that *in average*, the contribution to R_I and bdc of multiple pulses is equal to the sum of the contribution to R_I and bdc for each individual pulse.

Impact of the echoes generated by the first pulse on the second pulse of a pair: Since the DME/TACAN beacon emits pair of pulses, echoes generated by the first pulse could collide with the second pulse of the pair. This would be particularly problematic if the blanked interval generated by an echo directly collides with the blanked interval of the second pulse of the pair (impact on pw) or is nearer to the blanked interval of the second pulse than the blanked interval of the first pulse (impact of PW). However, this would require to have echoes triggering the blanker after a long additional travel time generating an additional delay $\tau_i^j > 6\ \mu s$ since the time interval between the two pulses of a pair is $12\ \mu s$. During this long additional travel time, the echoed signal is very attenuated

and it seems very unlikely to have an echo triggering the threshold with this additional delay. Therefore, this scenario is excluded from the R_I and bdc derivation considering multipath.

4.B. UPDATED NOTATION

In this subsections, a new notation concerning the instants of time where the pulse starts and stops to be blanked, is introduced.

Since LOS pulse is chosen to be centered at 0, echoed pulses are not. Therefore, the instants of time where a echo triggers the blanker (blanker activation interval limits) must be defined since Equation (6) can no longer be directly used. Let's consider an echo arriving at the receiver with an additional delay τ_i^j with respect with the LOS. From Equation (2), instantaneous power $p(t)$ of the echo is defined as:

$$p(t) = P_i^j e^{-\alpha(t-\tau_i^j)^2} \tag{18}$$

Where:

- P_i^j is the PEP of the echo at the antenna output,

To obtain the instants of time where an echo triggers the blanker, $p(t)$ is equalized to the blanking threshold T_h. The resolution of the equation yields two solutions:

$$p(t) = T_H \Leftrightarrow \begin{cases} w_{i,j}^l = \tau_i^j - \sqrt{\dfrac{\ln\left(P_i^j / T_h\right)}{\alpha}} \\ w_{i,j}^r = \tau_i^j + \sqrt{\dfrac{\ln\left(P_i^j / T_h\right)}{\alpha}} \end{cases} \tag{19}$$

Where $w_{i,j}^l$ is the instant of time the echo starts to trigger the threshold (the upper index "l" stands for left) and $w_{i,j}^r$ is the instant of time the echo stops to trigger the threshold (the upper index "r" stands for right).

4.C. bdc MATHEMATICAL MODEL CONSIDERING MULTIPATH

In this section, first a simple example, one LOS signal and one echo, from **Figure *7***, is presented to introduce the mathematical definitions, notions and elements necessary to define an updated pw and bdc formula considering multipath. Afterwards, these formulas are generalized to consider any potential combination of LOS and number of echoes.

Application to a simple case: From **Figure *7***, the total blanked interval I_i^{bdc} is no longer one interval created by the direct pulse but the combination of the blanked intervals generated by the direct and the echoed pulse. The blanked intervals generated by the direct and the echoed pulse are denoted $I_{i,1}^{bdc}$ and $I_{i,2}^{bdc}$ respectively. With these new notations, I_i^{bdc} is derived from:

$$I_i^{bdc} = I_{i,1}^{bdc} U I_{i,2}^{bdc} \tag{20}$$

Where:

$$\begin{cases} I_{i,1}^{bdc} = [w_{i,1}^l, w_{i,1}^r] \\ I_{i,2}^{bdc} = [w_{i,2}^l, w_{i,2}^r] \end{cases} \tag{21}$$

I_i^{bdc} can also be seen at the union of all the disjoint blanked intervals B_i^k. In the simple case presented **Figure 7**, they are two disjoint blanked intervals, which are directly equals to $I_{i,1}^{bdc}$ and $I_{i,2}^{bdc}$. With this new definition, I_i^{bdc} is derived from:

$$I_i^{bdc} = B_i^1 UB_i^2 \tag{22}$$

The above threshold pulse width pw is then simply retrieved by applying Equation (8):

$$pw = length\left(I_i^{bdc}\right) = length(B_i^1 UB_i^2) \tag{23}$$

Generalization to J_i echoes: Generalizing to a number J_i of echoes, the updated expression for I_i^{bdc} is:

$$I_i^{bdc} = \bigcup_{j=1}^{J_i} I_{i,j}^{bdc} = \bigcup_{k=1}^{K_i} B_i^k \tag{24}$$

Where:

- J_i is the number of echoes generated from source i,
- $I_{i,j}^{bdc}$ is the blanked intervals generated by the echo j of source i,
- K_i if the number of disjoint blanked intervals for source i, $K_i \leq J_i$
- B_i^k are the disjoint blanked intervals, retrieved from the list of $I_{i,j}^{bdc}$

From the new definition of I_i^{bdc}, the new formula for pw considering multipath is:

$$pw = length(I_i^{bdc}) = length\left(\bigcup_{k=1}^{K_i} B_i^k\right) \tag{25}$$

Which finally gives, from Equation (9), the bdc mathematical model now considering multipath:

$$bdc = 1 - e^{-2\sum_{i=1}^{N} length\left(\cup_{k=1}^{K_i} B_i^k\right)\cdot PRF_i} \tag{26}$$

4.D. R_I MATHEMATICAL MODEL CONSIDERING MULTIPATH

In this section, first a simple example, one LOS signal and one echo, from **Figure 7** is presented to introduce the mathematical definitions, notions and elements necessary to define an updated PW and R_I formula considering multipath. Afterwards, these formulas are generalized to consider any potential combination of LOS and number of echoes.

Application to a simple case: From **Figure 7**, there are two $PW_{i,pulse}$ that need to be derived. The one from the direct pulse, $PW_{i,pulse}^1$, and the one for the echoed pulse, $PW_{i,pulse}^2$. Both of these pulses are generating a blanked disjoint interval B_i^1 and B_i^2, which blanks part of their tails. Taking the example of $PW_{i,pulse}^1$, applying Equation (14) and stating that $\tau_i^0 = 0$ (the direct pulse has no additional delay) PW_i^1 is obtained as:

$$PW_{i,pulse}^1 = \int_{-\infty}^{-w_{i,1}^l} e^{-\alpha(t-\tau_i^0)^2} dt + \int_{w_{i,1}^r}^{w_{i,2}^l} e^{-\alpha(t-\tau_i^0)^2} dt + \int_{w_{i,2}^r}^{+\infty} e^{-\alpha(t-\tau_i^0)^2} dt \tag{27}$$

Now, in order to keep the same formalism from Equation (14), it is possible to rewrite this expression as:

$$PW_{i,pulse}^1 = \int_{-\infty}^{-w_{i,1}^l} e^{-\alpha(t-\tau_i^0)^2} dt + \int_{w_{i,1}^r}^{+\infty} e^{-\alpha(t-\tau_i^0)^2} dt - \int_{w_{i,2}^l}^{+\infty} e^{-\alpha(t-\tau_i^0)^2} dt + \int_{w_{i,2}^r}^{+\infty} e^{-\alpha(t-\tau_i^0)^2} dt \tag{28}$$

Which yields, applying $u = \sqrt{\alpha}(t - \tau_i^0)$ change of variable:

$$PW_{i,pulse}^1 = \frac{\sqrt{\pi/\alpha}}{2}\left[erfc\left(\sqrt{\alpha}|w_{i,1}^l - \tau_i^0|\right) + erfc\left(\sqrt{\alpha}|w_{i,1}^r - \tau_i^0|\right) - \left(erfc\left(\sqrt{\alpha}|w_{i,2}^l - \tau_i^0|\right) - erfc\left(\sqrt{\alpha}|w_{i,2}^r - \tau_i^0|\right)\right)\right] \tag{29}$$

Which is the $PW_{i,pulse}$ obtained without any multipath, with a removed part due to the blanked interval generated by the echoed pulse. Applying the exact same methodology for PW_i^2, we obtain:

$$PW_{i,pulse}^2 = \frac{\sqrt{\pi/\alpha}}{2}\left[erfc\left(\sqrt{\alpha}|w_{i,2}^l - \tau_i^1|\right) + erfc\left(\sqrt{\alpha}|w_{i,2}^r - \tau_i^1|\right) - \left(erfc\left(\sqrt{\alpha}|w_{i,1}^r - \tau_i^1|\right) - erfc\left(\sqrt{\alpha}|w_{i,1}^l - \tau_i^1|\right)\right)\right] \quad (30)$$

An interesting comment to make here is that the first $erfc$ removed in Equation (30) is the one starting at $w_{i,1}^r$ (right part of the blanked interval generated by the direct pulse) while the one added is the one starting at $w_{i,1}^l$ (left part of the blanked interval generated by the direct pulse). This is the opposite in Equation (29).

Therefore, from Equation (29) and Equation (30), two rules can be stated:

- The addition of a blanked interval B_i^k adds a double sum of $erfc$ functions to the PW derivation
- The sign of both these added $erfc$ functions depends on the position of the added blanked interval relatively to the pulse considered

<u>Generalization to J_i echoes</u>: Generalizing to a number J_i of echoes, the updated expression for PW is, from Equation (11):

$$PW_i = \sqrt{\pi/\alpha}\sum_{j=0}^{J_i} P_i^j \left[2\left(1 - 1_{I_i^{bdc}}(\tau_i^j)\right) + \sum_{k=1}^{K_i} \begin{array}{l} sign\left(\tau_i^j - B_i^{k,l}\right)^{1-1_{B_k}(\tau_i^j)} erfc\left(\sqrt{\alpha}|B_i^{k,l} - \tau_i^j|\right) + \\ +sign\left(B_i^{k,r} - \tau_i^j\right)^{1-1_{B_k}(\tau_i^j)} erfc\left(\sqrt{\alpha}|B_i^{k,r} - \tau_i^j|\right) \end{array}\right] \quad (31)$$

Where:

- J_i is the number of echoes generated by source i
- K_i is the number of disjoint blanked intervals generated by the J_i echoes of source i,
- $1_A(x)$ is the indicator function of the ensemble A, $1_A(x) = \begin{cases} 1\ if\ x \in A \\ 0\ otherwise \end{cases}$,
- P_i^j is the received power generated by the obstacle j,
- τ_i^j is the additional delay of echo j with respect to the direct pulse generated by source i.

Which finally gives, from Equation (15), the R_I mathematical model now considering multipath:

$$R_I = \sum_{i=1}^{N} \frac{SSC(\Delta f_i)PRF_i\sqrt{\pi/\alpha}}{N_0\beta_0} \cdot \left(\sum_{j=0}^{J_i} P_i^j \left[2\left(1 - 1_{I_i^{bdc}}(\tau_i^j)\right) + \sum_{k=1}^{K_i} \begin{array}{l} sign\left(\tau_i^j - B_i^{k,l}\right)^{1-1_{B_i^k}(\tau_i^j)} erfc\left(\sqrt{\alpha}|B_i^{k,l} - \tau_i^j|\right) + \\ +sign\left(B_i^{k,r} - \tau_i^j\right)^{1-1_{B_i^k}(\tau_i^j)} erfc\left(\sqrt{\alpha}|B_i^{k,r} - \tau_i^j|\right) \end{array}\right]\right) \quad (32)$$

4.E. IMPORTANT REMARK

A very important remark from both bdc and R_I mathematical models considering multipath is that to compute bdc, the length of the B_i^k must be derived, which implies the knowledge of the $w_{i,j}^l$ and $w_{i,j}^r$ and so τ_i^j and P_i^j (Equation (19)). τ_i^j and P_i^j are also directly used in the R_I computation. Therefore, to compute the C/N_0 degradation, **the precise knowledge of P_i^j and τ_i^j is necessary**. These values are often determined using a channel propagation model. The presentation of the proposed propagation channel model, specially adapted for the DME/TACAN interference analysis, is precisely the object of the next section.

5. PROPOSED PROPAGATION CHANNEL MODEL

As mentioned in the previous section, to be able to apply the C/N_0 degradation analytical model considering multipath, the precise knowledge of the received power P_i^j and the additional delay τ_i^j of the echoed pulse with respect to the direct ray is required to calculate the values of bdc and R_I. The objective of the propagation channel is thus to obtain these values from few information about the obstacles.

The scenarios investigated in this article and in future standards are scenarios where the aircraft is at a certain flight level (likely ≥ 2100 feet) which means that a high number of obstacles around many DME/TACAN stations must be considered. Therefore, on one hand, the propagation channel model proposed in this work is as simple as possible in order to deal with many obstacles without being too computationally expensive. On the other hand, the proposed channel model should be complex enough to provide a realistic impact of the multipath. The solutions and assumptions considered for the propagation channel derivation in order to reach the desired trade-off between simplicity and representativity are presented in the next subsections.

5.A. PRESENCE OF MULTIPATH

The first set of assumptions, namely the Radio Line Of Sight (RLOS), the shadowing phenomenon and the ground effect, concerns the determination of whether an obstacle present in the scenario reflects the direct signal or not. Indeed, considering the high number of DME/TACAN beacons potentially communicating with the aircraft, it is important to limit the number of obstacles reflecting the direct signal around these beacons while ensuring that the most threatening ones are not overlooked. These assumptions are presented in this subsection.

Radio Line Of Sight (RLOS): Only the obstacles that are in the Radio Line Of Sight (RLOS) horizon of the DME/TACAN beacons are kept as potential candidates to reflect the direct signal. Using an effective earth radius of $4/3R_T$, where R_T is the actual earth radius as depicted in ITU-R P834-9, (2017), the RLOS is formulated as:

$$RLOS = \sqrt{(4/3R_T + H_{DME})^2 - (4/3R_T)^2} + \sqrt{(4/3R_T + H)^2 - (4/3R_T)^2} \quad (33)$$

Where:

- R_T is the earth radius, $R_T = 6378{,}14\ km$
- H_{DME} is the height of the DME/TACAN beacon antenna,
- H is the height of the obstacle.

In the case of DME/TACAN, the height above ground of the beacon's antenna is usually 10 meters ($H_{DME} = 10\ m$). For example, with an obstacle's height of 10 meters ($H = 10\ m$), the RLOS is about $25\ km$.

Shadowing: A shadowing-phenomenon is also assumed in the model. This means that obstacles in the shadow of any other obstacles are not considered to reflect the direct signal (since it is assumed that the direct signal does not reach them). **Figure *8*** provides an example of this phenomenon, where the red obstacle does not reflect the direct signal because of the shadow created by the green obstacle.

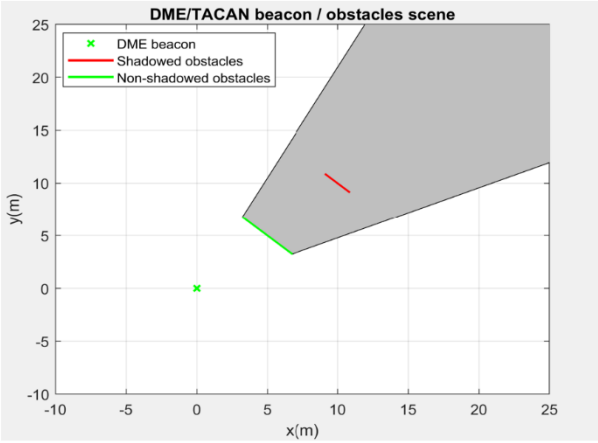

Figure 8: Representation of shadowing-phenomenon, upper view

Ground reflection: From simplification purpose, the ground reflection is not considered.

5.B. ASSUMPTIONS FOR THE ADDITIONAL DELAY τ_i^j CALCULATION

In this subsection, the assumptions used for the additional delay τ_i^j calculation, namely the first order of reflection and the earth flat assumption, are presented.

First order of reflection: To simplify the analysis, only the first order of reflection are considered, meaning that the obstacles can only reflect the ray coming from the DME/TACAN beacon's antenna.

Earth flat: For simplification purpose, the earth is considered flat in our study. Similarly, the earth relief is not considered.

5.C. EXPRESSION OF THE ADDITIONAL DELAY τ_i^j

Considering the previous assumptions, the formula of the additional delay τ_i^j of the echoes with respect with the LOS ray is the following:

$$\tau_i^j = \frac{R_1 + R_2 - D}{c} \tag{34}$$

Where:

- R_1 is the distance between the DME/TACAN beacon and the obstacle,
- R_2 is the distance between the obstacle and the aircraft,
- D is the distance between the DME/TACAN beacon and the aircraft (direct path),
- c is the speed of light.

5.D. ASSUMPTIONS FOR THE REFLECTED POWER P_i^j DERIVATION

In this subsection, the assumptions used for the reflected power P_i^j, namely the far-field propagation model and the obstacle material, are presented.

Far-field propagation model: The reflected power P_i^j derivation is made assuming a far-field propagation model, meaning that the obstacle must be in the far-field of the DME/TACAN beacon antenna and that the aircraft must be in the far-field of the obstacle. This was deemed necessary since the resolution of the Stratton-Chu integrals is much easier in that case, as depicted in Chen, (2011). An object A is in the far-field of an object B if:

$$R \geq \frac{2L^2}{\lambda} \tag{35}$$

Where:

- R is the distance between A and B,
- L is the largest dimension of object A,
- λ is the wavelength associated to the DME/TACAN carrier frequency by $\lambda = c/f_i$.

In the case of the link between the DME/TACAN antenna and the obstacle, the condition is always respected. Indeed, the maximum dimension L of the DME/TACAN is the antenna size. Indeed, in that case, L = 5m, $\lambda = 25.5cm$ (considering DME/TACAN emitting at exactly the L5 frequency) resulting in $R \geq$ 200m, and a distance shorter than 200m between the DME and an obstacle is unlikely since no obstacle should be found in a circle of radius 300m around the DME/TACAN beacon according the guidance of ICAO, (2015).

Concerning the link between the obstacle's center and the aircraft, the condition is more difficult to enforce since the maximum dimension L is now the dimension of the obstacle (that can reach a few hundred of meters). Therefore, to ensure that the far-field condition is always respected, not-far-field-complying obstacles are divided in smaller obstacles portions as much as needed such that every obstacle portion respects the far-field condition. The scattered electric field is then derived from every portion and the reflected power P_i^j is retrieved from the coherent sum of the electric field of each individual portion. **Figure *9*** provides an example of that process, where the initial obstacle is divided three times.

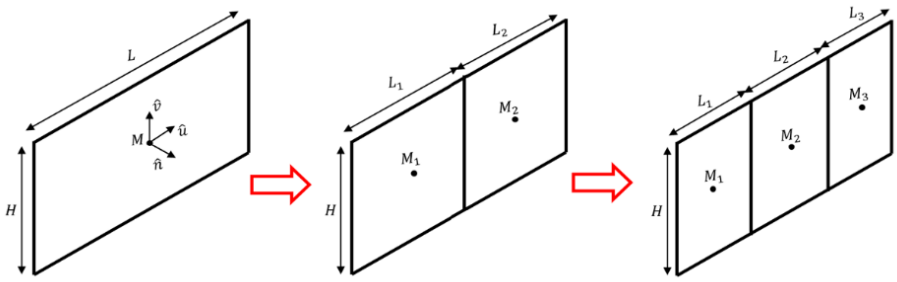

Figure 9: Example of the proposed methodology to ensure that the far-field condition is always respected (three divisions)

Obstacle material: The second assumption concerns the number of different available materials an obstacle can be made of, since the expression of the reflected power P_i^j depends on the obstacle's composition. For the sake of simplicity, while still being representative to real life scenarios, obstacles can be made of **one individual material among four different available materials**: metal, concrete, brick, and wood. The materials are modelized as a slab characterized by a thickness and a permittivity ϵ_r (values provided in **Table *1***).

5.E. EXPRESSION OF THE REFLECTED POWER P_i^j

In this subsection, considering the previous assumptions, the derivation of the reflected power P_i^j in the two following cases: when the obstacles are perfectly smooth, and when roughness is added to the surface, is conducted. Note that in this paper, the roughness term is used to characterize details such as windows, with dimension $\geq \lambda$, added to the obstacles.

General scheme: Figure *10* shows (a) the DME/TACAN beacon (represented by A), obstacle (represented by M) and aircraft (represented by B) scene in the spheric coordinate system and (b) a zoom on a perfectly smooth obstacle with center M, length L and height H.

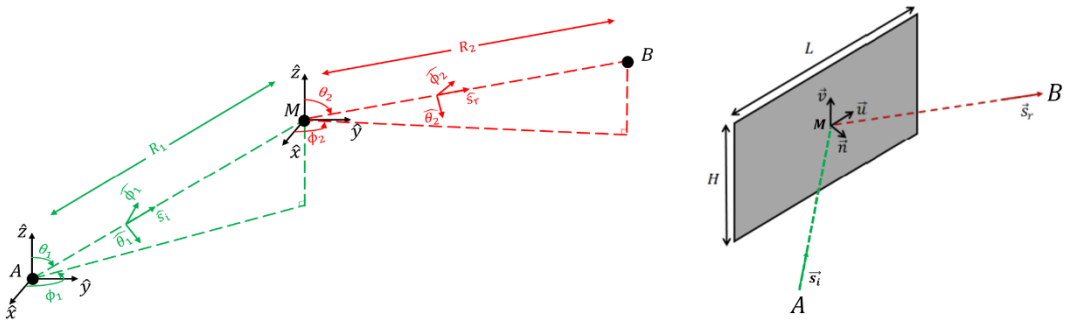

(a) (b)

Figure 10: Representation of (a) DME-Obstacle-Aircraft scene and (b) zoom on the perfectly smooth obstacle

From **Figure *10***, four useful definitions can be introduced:

- $\widehat{s_i}$ is the direction of incidence, $\widehat{s_i} = \frac{\overrightarrow{AM}}{||\overrightarrow{AM}||}$, where the DME/TACAN beacon antenna center is modelized A,
- $\widehat{s_r}$ is the direction of observation, $\widehat{s_r} = \frac{\overrightarrow{BM}}{||\overrightarrow{BM}||}$, where the aircraft antenna center is modelized by B,
- $\hat{n}$ is the normal vector to the obstacle,
- $\hat{u}$ and $\hat{v}$ are the unit vectors completing the orthonormal base.

In the most general case, the calculation of the Stratton-Chu integrals gives the following equation for the reflected power P_i^j:

$$P_i^j = \frac{P_{TX}G_{TX}(el_1)G_{RX}(el_2)}{(4\pi)^2 R_1^2 R_2^2}|R_{TE}|^2(LH)^2\, f(V,H)g(U,L)\cos(\phi_p - \phi_1)^2 \sin(\theta_2)^2 \quad (36)$$

Where:

- R_{TE} is the reflection coefficient (which depends on the material). The rationale to derive R_{TE} is presented in Chabory, (2004).
- P_{TX} is the transmitted power of the DME/TACAN beacon,
- G_{TX} is the gain of DME/TACAN beacon's transmitting antenna,
- G_{RX} is the gain of the receiving aircraft antenna,
- el_1 the elevation angle between the DME and the position of the obstacle center,
- el_2 is the elevation angle between the obstacle and the center of the aircraft antenna,
- L and H are respectively the length and the height of the obstacle,
- $V = (\widehat{s_r} - \widehat{s_i}).\hat{v}$,
- $U = (\widehat{s_r} - \widehat{s_i}).\hat{u}$,
- ϕ_1 is the azimuth angle between the DME/TACAN beacon and the obstacle,
- ϕ_p is the angle between $\hat{x}$ and $\hat{n}$,
- θ_2 is the θ angle from the spherical coordinate system between the obstacle and the aircraft,
- $\boldsymbol{f}$ and $\boldsymbol{g}$ are two functions that will be customized for the two cases presented in this subsection: when the obstacles are perfectly smooth, and when roughness is added to the surface.

Case when the obstacles are perfectly smooth: From **Figure 10**, and following the calculation of the Stratton-Chu integrals in the case of a perfectly smooth obstacle in the far-field condition conducted in Chen, (2011), the function f and g are perfectly solved as $sinc^2$ functions, such that the reflected power P_i^j in that case is:

$$P_i^j = \frac{P_{TX}G_{TX}(el_1)G_{RX}(el_2)}{(4\pi)^2 R_1^2 R_2^2}|R_{TE}|^2(LH)^2\, sinc^2\left(k_0\frac{VH}{2}\right) sinc^2(k_0\frac{UL}{2})\cos(\phi_p - \phi_1)^2\sin(\theta_2)^2 \qquad (37)$$

Where:

- k_0 is the wave number, $k_0 = \frac{2\pi}{\lambda}$.

Case when roughness is added to the obstacle: To improve the realism of the propagation channel model, the inclusion of windows to the facades of the obstacles is necessary since most of them represent houses or other non-flat/non-smooth buildings. Generally speaking, roughness is included in most propagation channel model thanks to the precise knowledge of the facades' roughness and by meshing the obstacles with rectangles in the order of λ. However, no such knowledge is available for the high number of obstacles used in the analyzed scenarios . Moreover, the computational power required to produce such a precise meshing on all these obstacles is too high and will upset simplicity objective set for the modelling of this propagation channel.

To cope with these difficulties, it is proposed to find a customization of f and g thanks to the study of a unique facade, representative of a middle-tall sized building. The analysis is conducted in FRME (Fortran Range Multipath Error), a propagation channel model specially created for GNSS multipath analysis, Chen, (2011). Since a unique facade is studied, the facade details are perfectly introduced. **Figure *11*** represents the studied facade, where the core material can be customized to be metal, concrete, brick or wood.

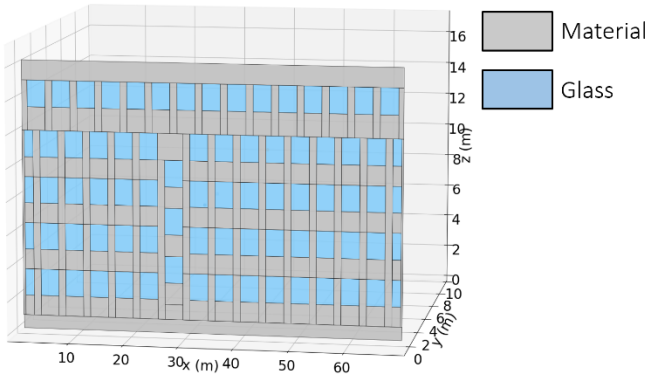

Figure 11: Representation of the studied facade

The objective of the study is to find two simple functions f and g such that the two sinc² functions from Equation (37) could be replaced to accurately introduce the details of the facade. From the observation of FMRE simulation results, it was observed that f and g were two sinc look-alike functions with:

1. Their highest peaks reduced
2. Never reaching zero
3. Having additional peaks that are Grating lobes created by the spatial periodicity of the windows
4. All previous observations depended on the obstacle material.

From these observations, function f and g are modelled as $sinc^2$ functions multiplied by a coefficient (< 1 except for wood), with the zeros removed (zeroes are replaced by the value of the nearest peak) and with a minimum value fixed at the maximum value of the periodicity peaks. f and g customized functions are called $sinc_{eq}^{vert}$ and $sinc_{eq}^{hor}$. Their mathematical models are:

$$\begin{cases} f(U,L) = sinc_{eq}^{hor}\left(k_0\frac{UL}{2}\right)^2 = K\cdot\max\left(sinc_{w0}\left(k_0\frac{UL}{2}\right),\left(\frac{M_{peak}^{hor}}{K}\right)\right)^2 \\ g(V,H) = sinc_{eq}^{vert}\left(k_0\frac{VH}{2}\right)^2 = K\cdot\max\left(sinc_{w0}\left(k_0\frac{VH}{2}\right),\left(\frac{M_{peak}^{vert}}{K}\right)\right)^2 \end{cases} \quad (38)$$

Where:

- K is the maximum of the electric scattered field obtained from the FMRE simulations,
- M_{peak}^{vert} and M_{peak}^{hor} are the maximum of the Grating lobes found in the electric scattered field from the FMRE simulations,
- $sinc_{w0}$ is defined as:

$$sinc_{w0}(x) = \max\left(sinc(x), sinc\left(\zeta(x)\right)\right) \quad (39)$$

Where:

$$\zeta(x) = \begin{cases} min(x_n \; such \; that \; x_n \geq |x|) \;\; \forall n \in [1,N] \;\; if \;\; |x| \leq x_N \\ x_N \;\; otherwise \end{cases} \quad (40)$$

With $(x_1, \ldots, x_N)$ the abscissa of the N first peaks of the $sinc$ function.

In total, eight $sinc_{eq}$ functions are determined, two per material. **Figure *12*** provides the example of the $sinc_{eq}^{hor}$ (in blue) compared with the true $sinc$ function (in orange) and the true f function (from FMRE) when windows are added (in green) for metal:

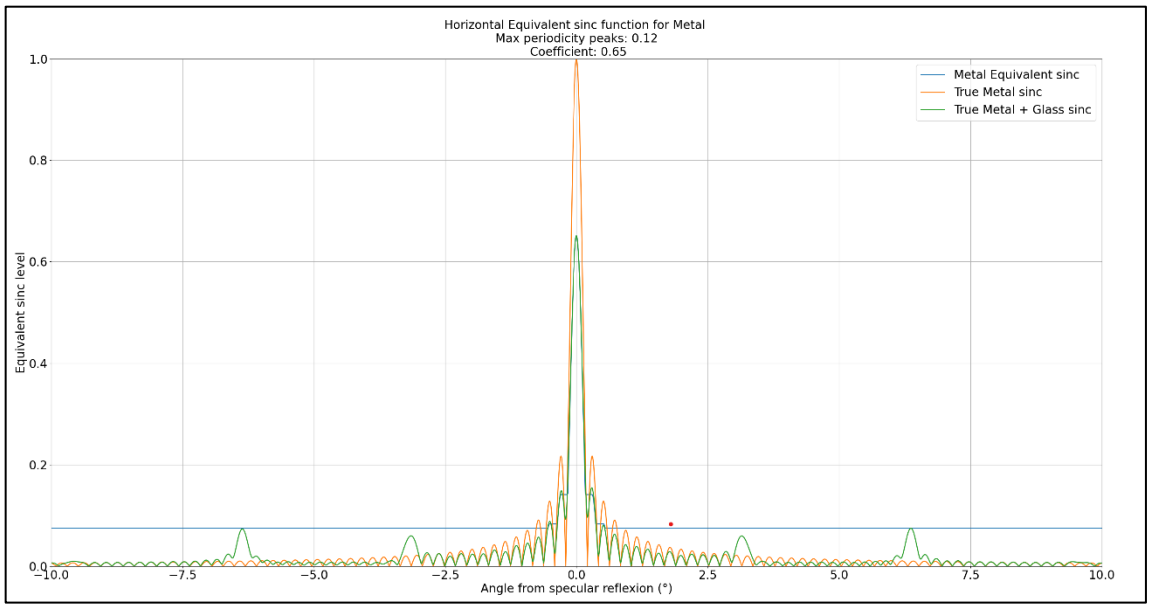

Figure 12: Representation of $sinc_{eq}^{hor}$ function for metal

From the new f and g functions, the new formula for Equation (36) considering the roughness of the obstacle is:

$$P_i^j = \frac{P_{TX}G_{TX}(el_1)G_{RX}(el_2)}{(4\pi)^2 R_1^2 R_2^2}|R_{TE}|^2(LH)^2 sinc_{eq}^{vert}\left(k_0\frac{VH}{2}\right)^2 sinc_{eq}^{hor}(k_0\frac{UL}{2})^2\cos(\phi_p-\phi_1)^2\sin(\theta_2)^2 \quad (41)$$

Where all the useful parameters to derive $sinc_{eq}^{vert}$ and $sinc_{eq}^{hor}$ for each of the material are provided in **Table 1**.

Table 1*: Parameters summary for $sinc_{eq}$ functions*

	Material	Permittivity (ϵ_r)	Max periodicity Peaks M_{peak}	Coefficient K
Horizontal sinc	**Metal**	–	0.078	0.65
	Concrete	6.5 –j0.4	0.0814	0.74
	Brick	3.75-j0.68	0.076	0.76
	Wood	1.42-j0.02	0.1296	1.44
Vertical sinc	**Metal**	–	0.2145	0.65
	Concrete	6.5 –j0.4	0.2294	0.74
	Brick	3.75-j0.68	0.2128	0.76
	Wood	1.42-j0.02	0.288	1.44

5.F. REMARK

Four obstacles' parameters are necessary to apply (41) and (37) reflected power formula:

1. The **position** of the center of the obstacles, that are needed to derive R_1, R_2 and many other parameters,
2. The **dimensions** L and H of the obstacles, that are directly used in the equations,
3. The **orientation** of the obstacles, which is used to derive ϕ_p,
4. The **composition** of the material, which is needed for the derivation of R_{TE} and both $sinc_{eq}^{vert}$ and $sinc_{eq}^{hor}$.

Knowing these four parameters, the value of the additional delay τ_i^j (Equation (34)) and the received power P_i^j (Equation (37) or (41)) can be retrieved for any obstacle. From τ_i^j and P_i^j, the value of R_I and bdc can be determined (Equation (32) and (26)) and finally the value of the C/N_0 computed (Equation (5)).

6. NUMERICAL APPLICATIONS

Now that the different models to determine the C/N_0 degradation in presence of multipath has been introduced, two numerical applications are introduced:

A. A comparison of the impact of multipath at low and at high altitude.
B. An application of the C/N_0 degradation model at a potential low-altitude US hot-spot, JALTO.

6.A. COMPARISON OF THE IMPACT OF MULTIPATH AT LOW AND HIGH ALTITUDE

In this subsection, the first numerical application of the propagation channel model and the C/N_0 degradation due to DME/TACAN only in presence of multipath is presented. After a presentation of the objective of the analysis, the methodology is introduced and further detailed. Finally, the results are presented and commented.

The objective of the first numerical application is to compare the impact of multipath at low and at high altitude flight levels. To achieve this objective, a single perfectly smooth metallic obstacle is considered for simplicity purposes. We are interested in the minimum area that is necessary to increase the above threshold pulse width pw by 50% (Equation (25)). Therefore, it is proposed to compare this minimum area at two Flight Levels (FL), FL21 and FL400 through six different scenarios. Note that this analysis is by no means exhaustive (other materials, flight levels and pw augmentations could have been investigated) but should provide a tendency on how the multipath impacts both low altitude and high altitude flight levels scenarios.

The 6 analyzed are defined as follows:

- The PEP of the DME/TACAN beacon, P_{TX}, is either 20 or 30 dBW, to accurately model approach-used DME/TACAN beacons ($P_{TX} = 20$ dBW) or en-route used DME/TACAN beacon ($P_{TX} = 30$ dBW).
- The Line Of Sight (LOS) received power PEP, P_{RX} is chosen to be either -90,-100 or -110 dBW, to accurately model direct pulses being largely, partially and moderately above the blanking threshold (-120dBW).
- The height H of the obstacles is always set to $10\ m$
- The blanking threshold is set to $-120\ dBW$

A summary of the 6 scenarios is provided **Table *2***.

Table 2*: Summary table of the 6 defined scenarios*

	$P_{TX}\ (dBW)$	$P_{RX}\ (dBW)$	$H\ (m)$	$T_H\ (dBW)$
Scenario 1	20	-90	10	-120
Scenario 2	20	-100	10	-120
Scenario 3	20	-110	10	-120
Scenario 4	30	-90	10	-120
Scenario 5	30	-100	10	-120
Scenario 6	30	-110	10	-120

The proposed methodology to obtain the minimum area for the 6 scenarios at the two FLs is as follows:

1. Determination of the distance D between the DME/TACAN beacon and the aircraft from P_{TX} and P_{RX} and FL
2. Determination of the **objective reflected peak envelope power** $P_i^{j,obj}$ necessary to reach the objective of having a pw increased by 50% for every additional delay τ_i^j, where τ_i^j varies from $0.264\ \mu s$ to 7,92 μs (3 times the rectangular equivalent width of a below-blanker pulse). Therefore, an initial candidate list of additional delays τ_i^j (values between $0.264\ \mu s$ to 7,92 μs) is defined and later processed in this step. This choice of values for τ_i^j is made to limit the obstacles' area obtained.
3. Determination of the obstacles' positions that generates τ_i^j values
4. Determination of the length L of the obstacles to reach $P_i^j = P_i^{j,obj}$ from P_{TX}, the obstacles, DME and aircraft positions.

Note that the multiplication of L by H, which has been arbitrary chosen to 10m for this study, gives the different areas needed to reach a value of pw increased by 50%.

<u>Determination of the distance *D*</u>: The distance D between the DME/TACAN beacon and the aircraft is chosen such that LOS received power P_{RX} is either -90,-100 or -110 dBW, given the scenario. D is retrieved from the free-space losses equation:

$$P_{RX} = P_{TX} G_{TX}(el) G_{RX}(-el) . \left(\frac{\lambda}{4\pi D^2}\right) \quad (42)$$

Where:

- el is the elevation angle between the DME/TACAN beacon and the aircraft

Determination of the objective reflected power $P_i^{j,obj}$: The objective power $P_i^{j,obj}$ needed to increase pw by 50% is found for every possible delay τ_i^j thanks to an algorithm testing every possible value of $P_i^{j,obj}$ starting at the blanking threshold T_H as its minimum value (pw is not increased if the echoed pulse does not trigger the blanker and thus has a power above the threshold) and ending at LOS received power P_{RX} as its maximum value (an echoed pulse cannot generate a power above the LOS power, unless for very specific cases that are outside the scope of this article).

For every tested $P_i^{j,obj}$, the values of the blanked instant of times $w_{i,2}^l$ and $w_{i,2}^r$ are determined from Equation (19). From $w_{i,2}^l$ and $w_{i,2}^r$ the blanked interval of the echoed pulse I_2^{bdc} is determined. From I_2^{bdc} and I_1^{bdc}, the disjoint blanked intervals can be determined and so pw (From Equation (25)). If for a specific additional delay τ_i^j, no objective power $P_i^{j,obj}$ valid value to increase pw by 50% is found (tested $P_i^{j,obj} \leq P_{RX}$), then this specific additional delay is removed from the candidate list of additional delay to investigate in the remaining steps of the methodology. Notes that the smaller the additional delay τ_i^j, the more difficult it is for the echoed pulse to increase pw by 50%.

Figure 13 (a) presents a graphical example of the objective power $P_i^{j,obj}$ for $P_{RX} = -117\ dBW$ (3dB above threshold) needed to increase pw by 50% with $\tau_i^j = 1.5\ \mu s$. **Figure 13** (b) presents an upper view of all $P_i^{j,obj}$ for every possible delay τ_i^j considering scenario 4 at FL21. Note that the blanked spots on the left of the DME/TACAN beacon and on the right of the aircraft are just aggregates due to the additional delay steps.

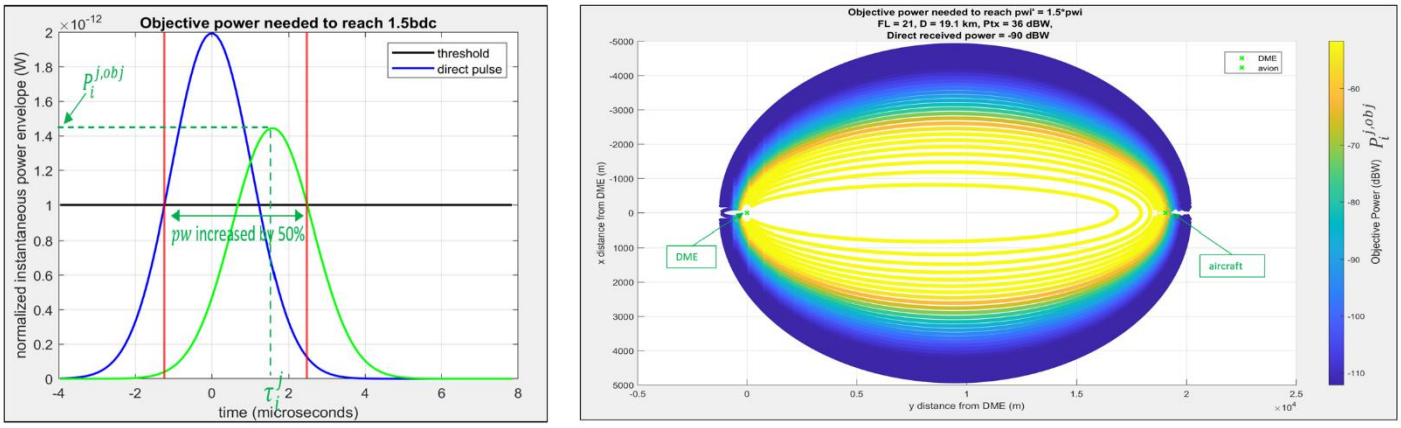

(a) (b)

Figure 13*:* Graphical example of (a) the objective power $P_i^{j,obj}$ for $P_{RX} = -117\ dBW$ needed to increase pw by 50% and (b) all the $P_i^{j,obj}$ for every possible delay τ_i^j considering scenario 4 at FL21

Determination of the obstacles' positions: All the obstacles' positions are defined such that an obstacle generates at least one of the targeted additional delays, τ_i^j, of the candidates list of additional delay generated in step 2. Three constraints must be additionally respected (if these 3 constraints are not respected, the obstacle position is not valid and discarded):

1. The obstacles must have a height $H = 10m$ (entry of the analysis).
2. The obstacles must respect the DME servitude.
3. The obstacles must respect the aircraft servitude.

For each individual delay τ_i^j, the obstacles' generating an additional delay τ_i^j are perfectly determined by an ellipsoid, with the following equation:

$$R_1 + R_2 = D + c \cdot \tau_i^j \tag{43}$$

Where:

- R_1 is the distance between the DME/TACAN beacon and the obstacle,
- R_2 is the distance between the obstacle and the aircraft,
- D is the distance between the DME/TACAN beacon and the aircraft (direct path),
- c is the speed of light.

To fulfill the first constraint, the intersection of the ellipsoid and the plan $z = H/2$ is determined. To respect the second constraint, the obstacles within a cylinder of radius $300m$ centered at the DME/TACAN beacons are excluded from the analysis (ICAO, 2015). To respect the third constraint, obstacles within a cylinder centered at the aircraft of radius $0.1\ nm$ (=$185.2\ m$) starting 150m above earth are excluded from the analysis.

Figure 14 shows (a) an example of an ellipsoid associated to an additional delay, with the two zones of servitude (in yellow) and the plan $z = H/2$ and (b) the resulting intersection of the ellipsoid with the plan.

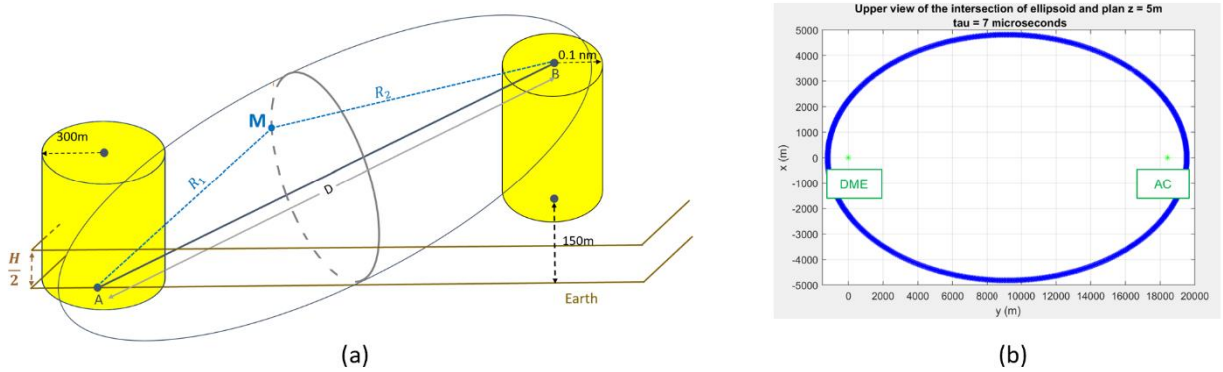

(a) (b)

Figure 14: Representation of (a) an ellipsoid and the two zones of servitude and (b) the intersection of this ellipsoid and the plan $z = H/2$

<u>Determination of the length *L*</u>: The last step of the methodology is to find the lengths L of the obstacles that generate a reflected power P_i^j equal to the objective power $P_i^{j,obj}$ necessary to increase pw by 50%, where P_i^j is obtained from Equation (37) (obstacles are assumed perfectly smooth).

Recall that to be able to use Equation (37), 4 parameters are needed:

- The **position** of the obstacles (which is known from the additional delay τ_i^j)
- The **dimensions** L and H of the obstacle. $H = 10m$ is known since it is on of the entries of the analysis.
- The **composition** of the obstacle which is known since the obstacles have been assumed to be perfectly metallic.
- The **orientation** of the obstacle.

Since the horizontal orientation ϕ_p of the obstacle is unknown, it is proposed to customize Equation (37) by computing the Cumulative Density Function (CDF) of $\psi(\phi_p)$ where ψ is the product of the two terms from Equation (37) that depends on the horizontal orientation:

$$\psi(\phi_p) = sinc\left(k_0 \frac{UL}{2}\right)^2 \cos\left(\phi_p - \phi_1\right)^2 \tag{44}$$

The 99^{th} quantile of that CDF, ψ_{99}, is then chosen in order to model a realistic worst-case scenario, excluding the case where the obstacle always generate a specular reflection (unrealistic worst-case scenario), but still having $\psi(\phi_p) < \psi_{99}$ 99% of the time.

The expression of the reflected power $P_i^{j,99}$ that depends on L can thus be expressed as:

$$P_i^{j,99}(L) = \frac{P_{TX} G_{TX}(el_1) G_{RX}(el_2)}{(4\pi)^2 R_1^2 R_2^2} |R_{TE}|^2 (LH)^2\ sinc^2\left(k_0 \frac{VH}{2}\right) \psi_{99} \sin(\theta_2)^2 \tag{45}$$

Multiple values of L, from 10 to 1000, are then tested to see if it is possible in this range of value to fulfil $P_i^{j,99} = P_i^{j,obj}$. If it is the case, the value of L is multiplied by H to obtain, for a given position, the area needed to increase pw by 50%. **Figure *15*** provides an example of the results obtained for the scenario 4 at FL21 where an upper view of the scene is represented. For each possible position, the value of the necessary area is represented by a color. The position is left blank if pw has not increased by 50% when $L = 1km$. The minimum area is surrounded by a red circle. Note that the discontinuities in the middle of the figure are only due to the step increase to speed up the process since it was noticed that less possible obstacles verifying $L < 1000\ m$ to increase pw by 50% were found in this area.

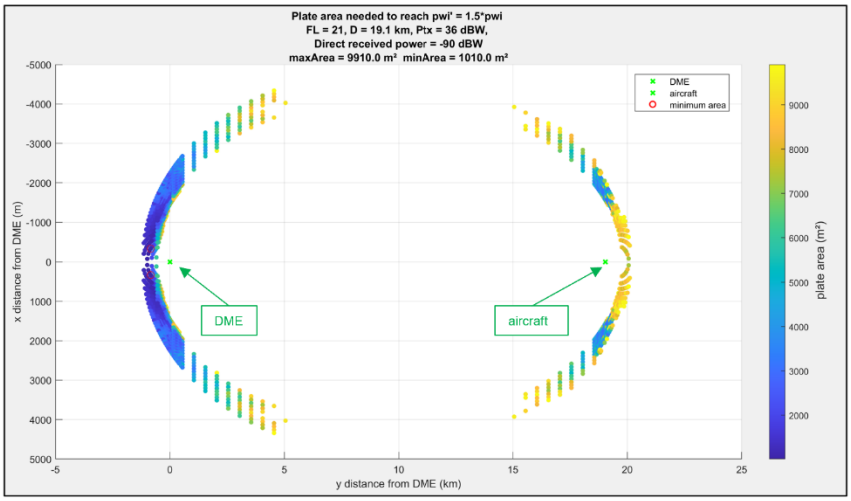

Figure 15:Upper view of the results for scenario FL21, $P_{TX} = 30\ dBW$, $P_{RX} = -90\ dBW$

The results of the minimum area for the 6 scenarios applied to FL21 and FL400 are presented in **Table *3***.

Table 3: *Results on the minimum area needed to increase pw by 50% for the 6 different scenarios*

	$P_{RX} = 20\ dBW$ $P_{TX} = -90\ dBW$	$P_{RX} = 30\ dBW$ $P_{TX} = -90\ dBW$	$P_{RX} = 20\ dBW$ $P_{TX} = -100\ dBW$	$P_{RX} = 30\ dBW$ $P_{TX} = -100\ dBW$	$P_{RX} = 20\ dBW$ $P_{TX} = -110\ dBW$	$P_{RX} = 30\ dBW$ $P_{TX} = -110\ dBW$
FL21	1200 m²	1000 m²	1200 m²	500 m²	600 m²	600 m²
FL400	> 10000 m²	3900 m²	9600 m²	3800 m²	4800 m²	3900 m²

From these results, it can be seen that it is more difficult to increase pw by 50% at high altitude (FL400) compared to low altitude (FL21), since the minimum area found at high-altitude is almost 4 times higher for every scenario. Therefore, it can be said, at least within the scope of this special application, that the impact of multipath is most significant at low-altitude FL.

6.B. APPLICATION TO JALTO, PHILADELPHIA

From a standardization point of view, the main concern brought by multipath impact is that the C/N_0 degradation generated by a low-altitude hot-spot exceeds the C/N_0 degradation already observed at Harrisburg, FL400. Indeed, the FL400 hotspot is determined as the location where the $C/N0_{eff}$ is the lowest one (as well as the location where the link budget margin is the smallest one) and thus the FL400 hotspot is the one driving the RFI compatibility mask (Garcia-Pena, Macabiau, et al., 2020). However, the $C/N0_{eff}$ calculation and specially the DME/TACAN bdc and R_I values were calculated without considering multipath impact.

The objective of the next application is precisely to tackle this question through the study of a potential low-altitude hot-spot, JALTO. JALTO has been chosen for two main reasons:

1. JALTO is a Final Approach Fix (FAF) waypoint where a lot of low altitude aircraft traffic is expected
2. JALTO is close to the original hot-spot of Harrisburg (FL400) where a lot of strong DME/TACANs pulses were observed

More specifically, the objective of this analysis is to determine a realistic over-bound of the C/N_0 degradation due to DME/TACANs only at JALTO considering multipath and to compare the over-bound with the one of the original hot-spot (7.34 dB). The original C/N_0 degradation due to DME/TACANs only at JALTO without any multipath is calculated to be equal to 2.29 dB.

The methodology to determine the targeted over-bound is the following:

1. Determination of the RLOS of the visible DME/TACAN beacons
2. Determination of the obstacles within the RLOS and some of their characteristics from a Microsoft publicly available database (positions, orientation and length)
3. Estimation of obstacles' composition through five different scenarios
4. Application of the C/N_0 degradation model

Determination of the RLOS of the visible DME/TACAN beacons:

19 DME/TACAN beacons are visible (inside the aircraft RLOS) from an aircraft flying at JALTO, dispatched in 5 different states:

- 6 in Pennsylvania
- 10 in New Jersey
- 1 in New York
- 1 in Delaware
- 1 in Maryland

Figure 16 shows a map of JALTO (in blue) and the DME/TACAN beacons (in red) in the 5 different states.

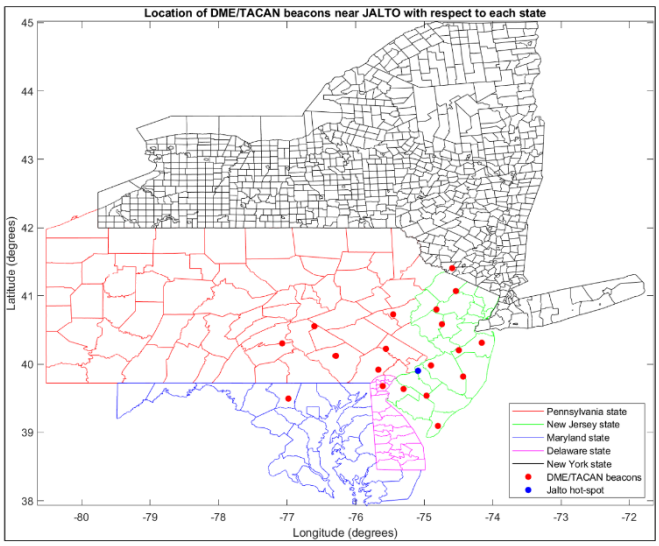

Figure 16: Map of JALTO and the DME/TACAN beacons in view

The RLOS of the 19 DME/TACAN beacons is obtained applying Equation (33). The height (H_{DME}) of the DME/TACAN beacons' antenna is retrieved from a 2018 Federal Aviation Administration (FAA) database, while the height H of the obstacles is arbitrary chosen to be 8 m. The mean of the RLOS obtained for the 19 DME/TACANs beacons is 24.73 km, with a very low standard deviation.

Determination of the obstacles within the RLOS:

The obstacles within the RLOS of the 19 DME/TACAN beacons are retrieved from a computer-generated and publicly available database of all the building footprints of the United released by Microsoft Maps, (2021). The building footprints from this database

have been digitalized using images that vary in date (from 2012 to 2021). In this database, the coordinates of the corners of each buildings are expressed in the WGS84 Coordinate Reference Systems (CRS). They are later expressed in the ENU coordinate system of all the visible DME/TACAN beacons for this special analysis. **Figure 17** presents an example of a building footprint extracted in that database.

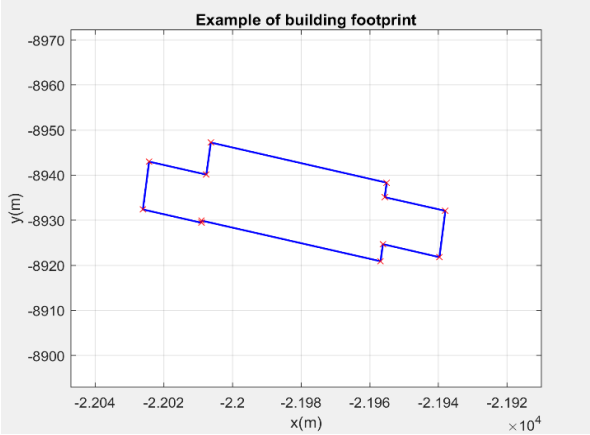

Figure 17: Example of building footprint extracted from the Microsoft Maps database

From the building footprints only, 3 important parameters needed to use the propagation channel model are retrieved: the position of the center, the length L and the horizontal orientation ϕ_p. Let's denote E and F the coordinates of two consecutive corners of a building:

- The **position** M of the center of the obstacles is simply retrieved by:

$$M = (F - E)/2 \tag{46}$$

- The **length** L of the obstacles is simply given by:

$$L = ||F - E||^2 \tag{47}$$

- The horizontal **orientation** ϕ_p is the angle between $\vec{x}$ and $\vec{n}$. Since $\vec{x}$ and $\vec{n}$ are unit vectors:

$$\phi_p = \begin{cases} \text{acos}(\vec{x}.\vec{n}) \; if \; \vec{n}.\vec{y} \geq 0 \\ 2\pi - \text{acos}(\vec{x}.\vec{n}) \; otherwise \end{cases} \tag{48}$$

From the positions, lengths and orientations of all the obstacles within the RLOS of all the DME/TACAN beacons, the shadowing phenomenon is applied resulting as a results in an exclusion of some of the obstacles inside the DME/TACAN RLOS. **Figure *18*** shows an example of the process of extracting the building footprint from the data base for the 11th DME/TACAN beacon with an upper view of (a) the Google Maps position of the beacon, (b) the extraction of the center of every obstacle within the RLOS where the color of each point represents the length of the obstacle and (c) the exact same plot after having applied the shadowing phenomenon.

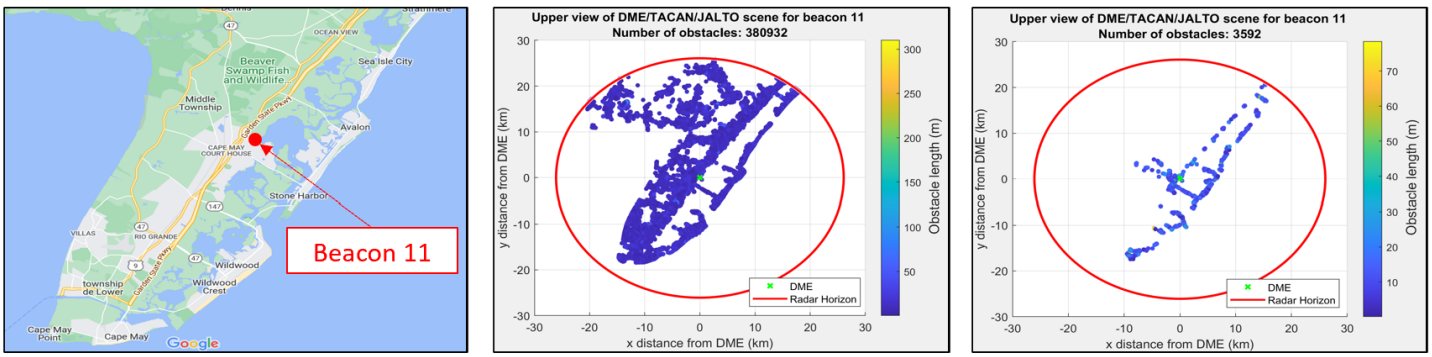

(a) (b) (c)

Figure 18: Example of methodology for beacon 11 with (a) the Google Map view, (b) the position and length of every obstacles extracted from the Microsoft database and (c) after having applied the shadowing phenomenon

Since the height H of the buildings were not publicly available from this database, it was arbitrarily decided to take $H = 8m$ for this analysis, which completes the **dimension** parameter for the application of the C/N_0 degradation.

Estimation of obstacles' composition through five different scenarios:
Since the composition of the materials was not directly given by the Microsoft database, in this analysis the composition is estimated through 5 different scenarios derived from the observation of the DME/TACAN beacons surroundings in Google Maps. A scenario is defined by the distribution (or percentage) of the obstacles' materials. **Table 4** provides the distribution proposed for the first 4 scenarios.

Table 4*: Material distributions for the 4 first scenarios*

	Length ≤ 50 m			**Length > 50 m**		
	Wood	**Concrete**	**Metal**	**Wood**	**Concrete**	**Metal**
Scenario 1	40%	40%	20%	40%	40%	20%
Scenario 2	45%	45%	10%	45%	45%	10%
Scenario 3	50%	50%	0%	0%	50%	50%
Scenario 4	50%	50%	0%	0%	70%	30%

In scenarios 1 and 2, there is no difference between the distribution for small ($L \leq 50m$) and large ($L > 50m$) obstacles. They are the simplest scenarios and the ones where the most metal obstacles are assumed to be present. Therefore, they should also be the worst-case scenarios. A small change is made on the metal composition distribution between these two scenarios.

In scenarios 3 and 4, a difference is made between small and large obstacles for the compositions of the materials. This was deemed necessary since it was found that the largest obstacles were made of concrete and metals (commercial centers, hospital, penitential center, etc.) whereas smaller obstacles were primarily made of a mix of concrete and wood (residential houses, small farms, etc.). A small change is made on the metal composition distribution between these two scenarios.

The scenario 5 is the most evolved one. It relies of the definition of 4 different zones:

- *Zone 1* is associated with large cities such as Philadelphia and Wilmington. Presence of large buildings. Dominance of concrete and brick.
- *Zone 2* is associated with normal-sized cities. Presence of many buildings. Dominance of wood and brick for small buildings and concrete and brick for large.
- *Zone 3* is associated with more rural areas such as allotment. Dominance of brick and wood.
- *Zone 4* is associated with coastal areas. Huge dominance of wood.

Table 5: *Summary of the distribution for the 4 different zones for the scenario 5*

	Length ≤ 50 m				**Length > 50 m**			
	Wood	**Concrete**	**Brick**	**Metal**	**Wood**	**Concrete**	**Brick**	**Metal**
Zone 1	45%	5%	45%	5%	2%	35%	55%	8%
Zone 2	55%	5%	35%	5%	5%	45%	45%	5%
Zone 3	65%	5%	25%	5%	8%	55%	35%	2%
Zone 4	80%	5%	10%	5%	20%	50%	15%	15%

In this scenario, each of the DME/TACAN beacons are assigned to a particular zone after a close observation of their surroundings. **Figure 19** presents the 19 DME/TACAN beacons associated with their particular zone, zone 1 being represented in red, zone 2 in yellow, zone 3 in green and zone 4 in blue.

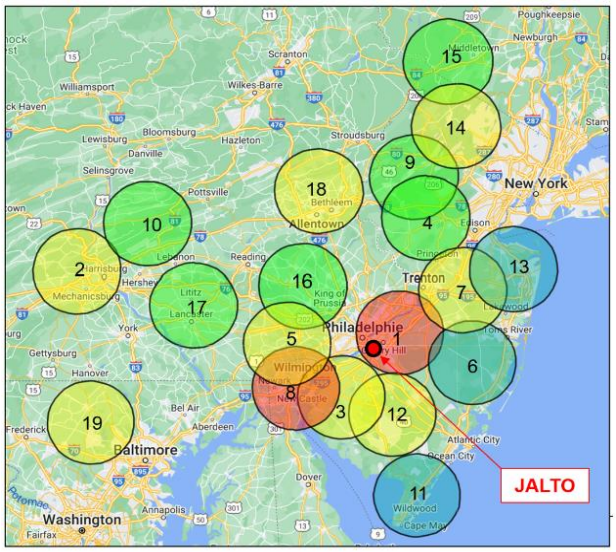

Figure 19: Representation of the 19 visible DME/TACAN beacons at JALTO within their different zones

The scenario 5 is the result of our finest estimation of the composition of the obstacles. It is the most realistic scenario of the 5 five scenarios defined despite still lacking the realism provided by an accurate database. Indeed, it must be noted that this scenario are best estimation efforts without any backing data except for detailed visual observations on Google maps.

<u>Application of the C/N_0 degradation model, results and conclusions</u>:

From the scenarios previously defined, we draw a material for each obstacles according to the distribution associated with the scenario. This allows to have the four necessary parameters to derive the additional delay τ_i^j and the reflected power P_i^j of all the obstacles in the RLOS of the 19 DME/TACAN beacons. From the additional delay τ_i^j and the reflected power P_i^j, a value for R_I, bdc and then the C/N_0 are determined. Since an aleatory component has been added to the model with the introduction of the scenarios, this process is repeated 1000 times for each scenario and the mean and standard deviation (std) of R_I, bdc and the C/N_0 degradation are determined. The results are presented in **Table *6***.

Table 6*: Results summary of the C/N_0 degradation at JALTO for the 5 different scenarios*

	R_I (-)		bdc (-)		C/N_0 degradation (dB)	
	Mean	**Std**	**Mean**	**Std**	**Mean**	**Std**
Scenario 1	1.8632	0.1494	0.3364	0.0108	6.3495	0.3011
Scenario 2	1.5800	0.1100	0.3268	0.0094	5.8348	0.2376
Scenario 3	1.0814	0.0831	0.3336	0.0055	4.9619	0.2058
Scenario 4	1.1494	0.0928	0.3291	0.0064	5.0565	0.2215
Scenario 5	1.3562	0.0881	0.3217	0.0084	5.4079	0.2028
Initial case	0.1664		0.3126		2.2964	

From **Table *6*** two conclusions can be made:

1. Even for the scenario 1, which is the scenario with the most metal obstacles (worst case scenario), the C/N_0 degradation due to DME/TACAN only found at JALTO including multipath does not exceed the original US hot spot found at Harrisburg, high altitude. Therefore, from these results, **it seems unlikely that a new low altitude hot-spot replaces the original US hot-spot**, even with the inclusion of multipath.

2. The C/N_0 degradation due to DME/TACAN only have been increased by at least 2.67 dB from the multipath-free theory in the 5 different scenarios. Therefore, **multipath seem to have a significant impact** on the C/N_0 degradation computation.

7. CONCLUSIONS

In the context of civil aviation, the RFI impact on a GNSS L5/E5a receiver is well characterized as the C/N_0 degradation observed at the receiver's correlator output, or equivalently, as an increase of the effective N_0 denoted as $N_{0,eff}$. In presence of a temporal blanker, $N_{0,eff}$ is derived from the blanker duty cycle bdc and the below-blanker interfering-signal-to-thermal-noise ratio R_I.

However, the model proposed RTCA, (2004) to derive both R_I and bdc does not include any consideration for multipath which could be problematic at low altitude. In this paper, the complete R_I, bdc and C/N_0 formulas have been reviewed and a new model considering multipath has been proposed. This new model requires the knowledge of precise time of arrival and received power of the echoed pulse. Therefore, a propagation model specifically adapted for the DME/TACAN interference analysis have also been proposed in this work.

This model has been developed to RFI-focused and to target the following trade-off: to be simple enough to be applied to a large number of scenarios with a high number of obstacles but to be complex enough to provide realistic estimations.

Two applications of the propagation channel model and the C/N_0 degradation computation considering multipath have been presented. The first one consists of a comparison of the impact of the inclusion of multipath in the C/N_0 degradation at high and at low altitude. The results shows that, for a single perfectly metallic obstacle, the impact at low altitude (FL21) is four time more significant than at high altitude (FL400). The second one is the study of a potential US low-altitude hot spot at JALTO, Philadelphia. Although the results tend to imply that it would be unlikely to find a new US hot-spot at low altitude due to the multipath, the impact of multipath is deemed significant since even the lowest C/N_0 degradation found considering multipath (4.96 dB) is 2.67 dB higher than the multipath-free theory (2.29 dB)

The main limitations to this work is the lack of real data containing DME/TACAN interferences as well as multipath, and the lack of information from the Microsoft database concerning multiple parameters of the obstacles (namely the height and the composition). This would need to be tackled in future works. Furthermore, an analysis on the C/N_0 degradation due to DME/TCAN only considering multipath of a potential European hot-spot, REDGO, Frankfurt, is to be conducted.

ACKNOWLEDGMENTS

The authors of this paper would like to deeply thank Davis Huerta C. for his contribution to this work.

REFERENCES

Chabory, A. (2004). *Modélisation Electromagnétique des radômes par des techniques basées sur les faisceaux gaussiens*. Paul Sabatier University, Toulouse, France

Chen, A. (2011). *Development of a Hybrid Deterministic-Statistical GPS Multipath Simulator for Airport Navigation* [PhD Thesis, Institut National Polytechnique de Toulouse].

Garcia-Pena, A., Julien, O., Gakne, P. V., Macabiau, C., Mabilleau, M., & Durel, P. (2019, September). *Efficient DME/TACAN Blanking Method for GNSS-based Navigation in Civil Aviation*. ION GNSS+ 2019, 32nd International Technical Meeting of the Satellite Division of The Institute of Navigation, Miami, Florida.

Garcia-Pena, A., Julien, O., Macabiau, C., Mabilleau, M., & Durel, P. (2020, January). GNSS C/N0 Degradation Model in Presence of Continuous Wave and Pulsed Interference. *ITM 2020, Navigation*.

Garcia-Pena, A., Macabiau, C., Novella, G., Julien, O., Mabilleau, M., & Durel, P. (2020, September). *In-band RFI GNSS L5/E5a Mask Definition*. ION GNSS+ 2020, 33rd International Technical Meeting of the Satellite Division of the Institute of Navigation, Virtual Event, United State.

ICAO. (2015). *European Guidance Material on Managing Building Restricted Aeras* (Third Edition).

ITU-R P834-9. (2017). *Effects of tropospheric refraction on radiowave propagation*.

Microsoft Maps. (2021). *US building footprints*. https://github.com/microsoft/USBuildingFootprints

RTCA. (2004). *DO-292 Assessment of Radio Frequency Interference Relevant to the GNSS L5/E5A Frequency Band*.